HHS Public Access

Author manuscript

Cell. Author manuscript; available in PMC 2018 January 12.

Published in final edited form as:

Cell. 2017 January 12; 168(1-2): 150–158.e10. doi:10.1016/j.cell.2016.12.009.

Inhibition of CRISPR-Cas9 with Bacteriophage Proteins

Benjamin J. Rauch[1,2], **Melanie R. Silvis**[1,3], **Judd F. Hultquist**[2,4,5], **Christopher S. Waters**[1,2], **Michael J. McGregor**[2,4,5], **Nevan J. Krogan**[2,4,5], and **Joseph Bondy-Denomy**[1,2,6]

[1]Department of Microbiology and Immunology, University of California, San Francisco, San Francisco, CA 94158, USA

[2]Quantitative Biosciences Institute, QBI, University of California, San Francisco, San Francisco, CA 94158, USA

[3]Tetrad Graduate Program, University of California, San Francisco, San Francisco, CA 94158, USA

[4]Department of Cellular and Molecular Pharmacology, University of California, San Francisco, San Francisco, CA 94158, USA

[5]J. David Gladstone Institutes, San Francisco, CA 94158, USA

SUMMARY

Bacterial CRISPR-Cas systems utilize sequence-specific RNA-guided nucleases to defend against bacteriophage infection. As a counter-measure, numerous phages are known that produce proteins to block the function of Class 1 CRISPR-Cas systems. However, currently no proteins are known to inhibit the widely used Class 2 CRISPR-Cas9 system. To find these inhibitors, we searched *cas9*-containing bacterial genomes for the co-existence of a CRISPR spacer and its target, a potential indicator for CRISPR inhibition. This analysis led to the discovery of four unique type II-A CRISPR-Cas9 inhibitor proteins encoded by *Listeria monocytogenes* prophages. More than half of *L. monocytogenes* strains with *cas9* contain at least one prophage-encoded inhibitor, suggesting widespread CRISPR-Cas9 inactivation. Two of these inhibitors also blocked the widely used *Streptococcus pyogenes* Cas9 when assayed in *Escherichia coli* and human cells. These natural Cas9-specific "anti-CRISPRs" present tools that can be used to regulate the genome engineering activities of CRISPR-Cas9.

Graphical Abstract

*Correspondence: joseph.bondy-denomy@ucsf.edu.
[6]Lead Contact

AUTHOR CONTRIBUTIONS

B.J.R., M.R.S., J.F.H, and J.B.D. designed the experiments; B.J.R., M.R.S., J.F.H, C.W., and M.J.M. prepared strains and performed experiments; N.J.K and J.B.D. supervised experiments; B.J.R. and J.B.D. wrote the manuscript with input from all authors.

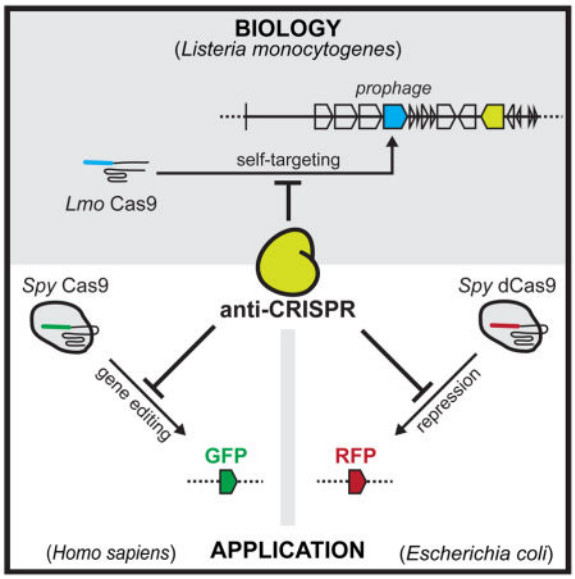

Four CRISPR-Cas9 inhibitor proteins encoded by *Listeria monocytogenes* prophages prevent Cas9 binding and gene editing in bacteria and human cells, including currently the most widely used Cas9 from *Streptococcus pyogenes*.

Keywords

CRISPR-Cas; Cas9; dCas9; anti-CRISPR; *Listeria* monocytogenes; bacteriophage; prophage; gene editing; Cas9 inhibitor

INTRODUCTION

The ability to prevent attack from viruses is a hallmark of cellular life. Bacteria employ multiple mechanisms to resist infection by bacterial viruses (phages), including restriction enzymes and CRISPR-Cas systems (Labrie et al., 2010). CRISPR arrays consist of the DNA remnants of previous phage encounters (spacers), located between Clustered Regularly Interspaced Short Palindromic Repeats (Mojica et al., 2005). These spacers are transcribed to generate CRISPR RNAs (crRNAs) that direct the binding and cleavage of specific nucleic acid targets (Brouns et al., 2008; Garneau et al., 2010). The CRISPR-associated (cas) genes required for immune function are often found adjacent to the CRISPR array (Marraffini, 2015; Wright et al., 2016). Cas proteins perform many functions, including destroying foreign genomes (Garneau et al., 2010), mediating the acquisition of foreign sequences into the CRISPR array (Nuñez et al., 2014; Yosef et al., 2012) and facilitating the production of mature CRISPR RNAs (crRNAs) (Deltcheva et al., 2011; Haurwitz et al., 2010).

CRISPR-Cas adaptive immune systems are both common and diverse in the bacterial world. Two distinct classes, encompassing six CRISPR types (I–VI) have been identified across bacterial genomes (Abudayyeh et al., 2016; Makarova et al., 2015), each with the ability to cleave target DNA or RNA molecules with sequence specificity directed by the RNA guide. The facile programmability of CRISPR-Cas systems has been widely exploited, opening the

door to an array of novel genetic technologies, most prominently gene editing in animal cells (Barrangou and Doudna, 2016). Most technologies are based on Cas9 (Class 2, type II-A) from *Streptococcus pyogenes* (Spy), together with an engineered single guide RNA (sgRNA) because of the simplicity of the system (Jinek et al., 2012). Gene editing in animal cells has been successful with Spy Cas9 (Cong et al., 2013; Mali et al., 2013), Cas9 orthologs within the II-A subtype (Ran et al., 2015), and new Class 2 single protein effectors such as Cpf1 (Type V (Zetsche et al., 2015)). Applications are also being developed through the characterization of Type VI CRISPR-Cas systems, represented by C2c2, which naturally cleave RNA (Abudayyeh et al., 2016; East-Seletsky et al., 2016). In contrast, the complex Class 1 CRISPR-Cas systems (Type I, III, and IV), consisting of RNA-guided multi-protein complexes and thus have been overlooked for most genomic applications. These systems are, however, the most common in nature, comprising ~75% of all bacterial CRISPR-Cas systems and nearly all systems in archaea (Makarova et al., 2015).

In response to the bacterial war on phage infection, phages, in turn, often encode inhibitors of bacterial immune systems that enhance their ability to either lyse their host bacterium or integrate into its genome (Samson et al., 2013). The first examples of phage-encoded “anti-CRISPR” proteins came for the Class 1 type I-F and I-E systems in *Pseudomonas aeruginosa* (Bondy-Denomy et al., 2013; Pawluk et al., 2014). Remarkably, ten type I-F anti-CRISPR and four type I-E anti-CRISPR genes have been discovered to date (Pawluk et al., 2016), all of which encode distinct, small proteins (50–150 amino acids), previously of unknown function. Our biochemical investigation of four I-F anti-CRISPR proteins revealed that they directly interact with different Cas proteins in the multi-protein CRISPR-Cas complex to prevent either the recognition or cleavage of target DNA (Bondy-Denomy et al., 2015). Anti-CRISPR proteins have distinct sequences (Bondy-Denomy et al., 2013), structures (Maxwell et al., 2016; Wang et al., 2016), and modes of action (Bondy-Denomy et al., 2015). These findings support the independent evolution of CRISPR-Cas inhibitors and suggests that many more are yet to be discovered. Indeed, a recent investigation exploited the conservation of signature anti-CRISPR associated (*aca*) gene with a predicted helix-turn-helix (HTH) motif to identify anti-CRISPRs across proteobacteria, broadly spanning the type I-F CRISPR-Cas phylogeny (Pawluk et al., 2016).

Although anti-CRISPRs are both prevalent and diverse within proteobacteria, it is presently unknown whether anti-CRISPR proteins occur in other bacterial phyla. Likewise, it is also unclear if anti-CRISPRs exist for systems other than types I-E and I-F. In *P. aeruginosa*, type I anti-CRISPRs are expressed from integrated phage genomes (prophages) and caused the constitutive inactivation of the host CRISPR-Cas system (Bondy-Denomy et al., 2013). In such cases the prophage can possess a DNA target with perfect identity to a CRISPR spacer in the same cell, as the CRISPR-Cas system is inactivated. The genomic co-occurrence of a perfect spacer and its target DNA is called “self-targeting” (Figure 1A). Bacteria with self-targeting require CRISPR-Cas inactivation for survival: in the absence of anti-CRISPR genes, the host genome will be cleaved in the act of targeting the prophage (Bondy-Denomy et al., 2013; Edgar and Qimron, 2010). Expression of an anti-CRISPR, therefore, neutralizes this risk. We surmised that genomes possessing a CRISPR system with apparent self-targeting would be candidates for the identification of new CRISPR-Cas inhibitors. Here, we describe the identification of four previously unknown phage-encoded CRISPR-Cas9

inhibitors in *Listeria monocytogenes* using a bioinformatics approach to identify incidents of self-targeting. We also demonstrate that two of these inhibitors can block the activity of *S. pyogenes* Cas9 in bacterial and human cells.

RESULTS

CRISPR-Cas9 in *Listeria monocytogenes* targets foreign DNA

Listeria monocytogenes is a facultative intracellular food-borne pathogen with a well characterized phage population. Many *L. monocytogenes* isolates have type II-A CRISPR-Cas systems (Sesto et al., 2014) and their CRISPR spacers possess identity to many virulent, temperate, and integrated phages (Di et al., 2014; Sesto et al., 2014). However, there is no experimental evidence of canonical CRISPR-Cas function. We analyzed 275 genomes of *L. monocytogenes* and identified type II-A CRISPR-Cas9 systems (Lmo Cas9) in 15% (n = 41) of them (Figure 1B). Interestingly, we found eight genomes (3% of the total), with examples of self-targeting (ST; Figure 1B and 1C and Table S1), although the CRISPR-Cas9 system is anticipated to be functional as all requisite genes are present with no obvious mutations (Figure S1A). Many self-targeted protospacers were found in prophages, and thus we predicted that these prophages encode inhibitors of CRISPR-Cas9 that allow the stable co-existence of a spacer-protospacer pair.

To test whether inhibitors were encoded by the prophages of *L. monocytogenes*, we first established the functionality of CRISPR-Cas9 in an *L. monocytogenes* strain (10403s) that does not exhibit self-targeting. To test the activity of this system we designed a plasmid (pT) possessing a targeted protospacer (i.e. a sequence that is complementary to a natural spacer in the CRISPR array) along with a cognate protospacer adjacent motif (PAM), a three base motif that is necessary for Cas9 binding (Figure 2A). We measured the transformation efficiency of 10403s with either pT or a control plasmid possessing a non-targeted sequence with an identical plasmid backbone (pNT). Transformation with pT yielded miniscule colonies relative to pNT (Figure 2B, leftmost panel), although the number of colonies that emerged upon prolonged incubation were the same (see Discussion for further analysis). To determine whether the 10403s prophage (ϕ10403s) was inhibiting CRISPR-Cas9 function in any way, a prophage-cured version of this strain (ϕcure) was tested, yielding the same tiny colonies (Figure 2B). The ϕcure strain was used for all subsequent experiments since it was indistinguishable from wt10403s in this assay. To confirm that the observed transformation inhibition was the result of CRISPR-Cas9 interference, we constructed a *cas9*-deletion strain. Transformation of this strain with pT and pNT produced colonies of indistinguishable size (Figure 2B). However, adding back *cas9* to the *L. monocytogenes* chromosome under a constitutively active promoter completely prevented transformation with pT (Figure 2B, rightmost panel). Together, these experiments demonstrate that Cas9 is functional in *L. monocytogenes* 10403s at both endogenous and overexpressed levels, and limits transformation with a plasmid bearing a protospacer.

Resident prophages inactivate CRISPR-Cas9 in *L. monocytogenes*

To determine whether CRISPR-Cas9 may be disabled in a strain with self-targeting spacers, we examined immunity function in *L. monocytogenes* strain J0161, whose spacer 16

perfectly matches a prophage (ϕJ0161a) in the same genome (Figure 1C). We could not detect any clearly deleterious CRISPR-Cas mutations in the CRISPR repeat, PAM, tracrRNA, Cas9, and the associated promoters of strain J0161 (Figures S1B-F and S2), suggesting that this self-targeting scenario was the result of inhibition and not loss of function. Since the type II-A CRISPR array of J0161 is distinct from that of 10403s, a J0161-specific targeted plasmid (pT_{J0161}) was used to test the function CRISPR-Cas9 in J0161. Consistent with the inactivation implied by self-targeting, there were no significant differences in transformation efficiency or colony size to distinguish pT_{J0161} from pNT (Figure 2C). Thus, we reasoned that the J0161 genome may encode Cas9 inhibitors.

In search of the genetic basis for CRISPR-Cas9 inactivation in J0161, we focused on the prophage ϕJ0161a as a likely source of an inhibitor gene because it contained the self-targeted sequence in this strain. To determine whether ϕJ0161a contained an inhibitor, the prophage-cured strain of 10403s was lysogenized with ϕJ0161a and assayed for CRISPR-Cas9 functionality by plasmid transformation (Figure 2D). The acquisition of ϕJ0161a was sufficient to inactivate CRISPR-Cas9 function (Figure 2E, left panels), suggesting that this prophage encodes an inhibitor of CRISPR-Cas9. The ϕJ0161a prophage also inactivated plasmid targeting in a strain constitutively expressing *cas9*, suggesting that the inhibitory mechanism does not operate by disrupting natural regulation of the *cas9* promoter (Figure 2E, right panels).

Given that the ϕJ0161a prophage inhibited CRISPR-Cas9 function in 10403s, and the endogenous ϕ10403s prophage did not, we compared the genomes of these two closely related phages to identify the regions of difference (Figure 3A). In addition to sharing 39 core phage genes with >40% protein sequence identity, ten non-overlapping unique clusters of genes were identified (cluster boundaries were chosen based on predicted operon structure, with 1–12 genes per cluster). Each cluster was cloned and integrated into the genome of prophage-cured 10403s and assayed for CRISPR-Cas9 function. Of the ten fragments, seven were successfully introduced into *L. monocytogenes*, while three fragments could not be inserted in the *L. monocytogenes* genome and were presumably toxic in isolation. Plasmid transformation assays revealed that ϕJ0161a fragment 1 was the only fragment capable of inhibiting CRISPR-Cas9, indicating that this fragment encoded at least one CRISPR-Cas9 inhibitor (Figure 3B). Expressing the individual genes from this four-gene fragment led to the conclusive identification of two anti-CRISPR genes, LMOG_03146 and LMOG_03147 (herein referred to as *acrIIA1* and *acrIIA2*, respectively) while LMOG_03145 and LMOG_03148 (*orfB* and *orfA*, respectively) had no anti-CRISPR activity (Figure 3B). Deletion of both *acrIIA1* and *acrIIA2* from a 10403s::ϕJ0161a lysogen restored CRISPR-Cas9 function, confirming that these are the only anti-CRISPR genes in ϕJ0161a (Figure 3B, rightmost panels).

Anti-CRISPR genes are widespread in *L. monocytogenes* prophages

To identify additional type II-A anti-CRISPRs, we examined the genomic position analogous to that of *acrIIA1* and *acrIIA2* in related *L. monocytogenes* prophages. A recurring anti-CRISPR (*acr*) locus containing *acrIIA1* within a small operon (2–5 genes) of highly conserved gene order was identified between the “left” integration site and the genes

involved in cell lysis (Figure 4A). We identified five additional protein families conserved within *acr* loci. To test these families for anti-CRISPR function, we cloned and integrated representatives into the 10403s genome and assayed for transformation efficiency of pT and pNT. Two new genes were identified that were capable of CRISPR inactivation (*acrIIA3* and *acrIIA4*), while the remaining three (*orfC, D, E*) were not (Figure 3C, Figure S3).

To determine whether CRISPR-Cas9 inactivation in *L. monocytogenes* is pervasive, we next analyzed the conservation pattern for each anti-CRISPR. Although each *acrIIA* gene was sufficient to inactivate CRISPR-Cas9 in isolation, we observed a common presence of *acrIIA1* in most *acr* loci. Nearly all instances (88%) of *acrIIA2-4* were found upstream of the helix-turn-helix (HTH) motif-containing *acrIIA1*, suggesting that this gene may be a marker for *acr* loci (Figure 4A and 4B). The most common scenario in 119 *acr* loci was either *acrIIA1-2* or *acrIIA1-2-3*, together representing 66% of *acr* loci (Figure 4B). In total, *acrIIA* genes were identified in 25% of *L. monocytogenes* genomes, with 53% of *L. monocytogenes cas9*-containing strains possessing at least one anti-CRISPR in the same genome (Figure 4C). Many instances of *L. monocytogenes* genomes possessing multiple *acrIIA*-encoding prophages were also identified (Supplementary Table 1). Furthermore, at least one *acrIIA* gene was found in the genomes of all eight instances of self-targeting that were initially identified (Figure 1B, Supplementary Table 1), explaining how these scenarios are stable. Together, these data suggest widespread prophage-mediated inactivation of CRISPR-Cas9 in *L. monocytogenes.*

Previous HTH-containing anti-CRISPR associated (*aca*) genes were used as markers to identify novel type I anti-CRISPR genes (Pawluk et al., 2016), although the *aca* genes did not have anti-CRISPR activity themselves. We hypothesized that *acrIIA1* could fulfill the role of such a marker. A comprehensive phylogenetic analysis of *acrIIA1* revealed that homologs were conserved widely across Firmicutes, in both mobile elements and core genomes (Figure 5A). A family of distantly related *acrIIA1* homologs was identified in *Listeria* genomes, as exemplified by the *orfD* gene, which had been independently identified as an *acr* locus member that also occurs upstream of *acrIIA4* homologs in contexts outside of prophages (Figure 4A and Table S1). While *orfD* lacked anti-CRISPR activity in a functional assay (Figure 3B), its co-occurrence with a *bona fide acr* gene suggests that the broad *acrIIA1/orfD* superfamily could be used as a marker to identify new *acr* genes. Future work will be necessary to determine whether the HTH-containing genes in these systems serve as effective markers for novel anti-CRISPR discovery.

To determine the homology landscape of *acrIIA2-4*, additional phylogenetic analyses were performed. Unlike *acrIIA1*, which was widespread across Firmicutes core genomes, the other three *acr* genes were mostly restricted to prophages in *Listeria*. Three distinct sequence families of *acrIIA2* were identified, all restricted to *Listeria* siphophages (a family of longtailed, non-contractile phages) (Figure 5B), while two *acrIIA3* families were observed in the genomes of siphophages infecting *Listeria* and *Streptococcus* (Figure 5C). Lastly, *acrIIA4* was observed in two distinct sequence families, one in *Listeria* siphophages and plasmids, and the other in a group of obligate virulent myophages (long contractile-tailed phages) (Figure 5D). While *acrIIA2* and *acrIIA3* were nearly always found with *acrIIA1*, *acrIIA4* often occurred in the absence of *acrIIA1* homologs in phages and mobile elements

of *Listeria*. For example, the family of *acrIIA4* in virulent phages are distinct from the other family of *acrIIA4* homologs in that they have an ~70 amino acid C-terminal extension in the predicted protein and do not occur with the HTH-containing genes *acrIIA1* or *orfD*, suggesting potential mechanistic and evolutionary distinctions between these *acrIIA4* families. Together, these analyses reveal ample sequence space for surveying homologous *acr* genes for specificity determinants and suggest an active arms race between *cas9* and mobile elements in *L. monocytogenes.*

AcrIIA2 and AcrIIA4 inhibit *S. pyogenes* Cas9

To determine the versatility of the Lmo Cas9 AcrIIA proteins, we asked whether these inhibitors were functional on the related Cas9 protein from *S. pyogenes* (Spy, 53% identical to Lmo Cas9). This ortholog has been used widely for biotechnological applications as an RNA-guided nuclease (Barrangou and Doudna, 2016), as well as for programmable gene repression by a catalytically deactivated mutant (dCas9) (Gilbert et al., 2013; Qi et al., 2013). Using an *E. coli* strain that carries Spy dCas9, we tested whether AcrIIA proteins block dCas9 from interfering with transcription of a chromosomal RFP reporter gene (Figure 6A). In a genetic background lacking inhibitors, the presence of an sgRNA and dCas9 reduced RFP fluorescence ~40-fold (2.6% relative to that of a strain with no sgRNA). *acrIIA1* had no impact on dCas9-mediated transcriptional repression, nor did *orfA*, *orfC*, or *orfD*, negative controls that had no anti-CRISPR activity in *L. monocytogenes. acrIIA2* partially blocked dCas9 function, with fluorescence reduced only 4-fold (25% relative to the no guide control), while *acrIIA4* nearly completely blocked dCas9, with fluorescence at 85% of the no guide control (Figure 6B). We could not obtain meaningful data from *acrIIA3* because the protein was toxic to *E. coli*. This lowered the recorded cell count during flow cytometry (see Figure S4a) and lead to large variability in the fluorescence measurements. A homolog of *acrIIA3* from *S. pyogenes* (accession number: AND04610.1) with 45% sequence identity to Lmo_*acrIIA3* was tested, but also resulted in impaired growth of *E. coli* (Figure S4b). The mechanism of *acrIIA3* toxicity in *E. coli* remains to be determined. We conclude that the *acrIIA2* and *acrIIA4* inhibit Spy dCas9 in *E. coli* to different degrees.

Given the common application of Spy Cas9 in eukaryotic cells, we next tested the AcrIIA proteins for their ability to block gene editing in human cells. HEK293T cells with an inducible, chromosomally-integrated eGFP reporter gene were transiently transfected with a plasmid expressing both Spy Cas9 and an sgRNA targeting eGFP in the presence or absence of vectors expressing human codon optimized *acrIIA* genes. After allowing gene editing to proceed for 36 h, eGFP was induced for 12 h, and cellular fluorescence was then measured by flow cytometry (Figure 6C). In the presence of Cas9 and the eGFP sgRNA, gene editing resulted in a 25% decrease in the number of GFP positive cells, while co-expression with *acrIIA2* or *acrIIA4* prevented Cas9-based gene editing (Figure 6D). We additionally tested the *S. pyogenes* homolog of *acrIIA3* (Spy_*acrIIA3*), which was not toxic in human cells, but it had no impact on Cas9 function in this assay. *acrIIA1* was non-functional in human cells, as was the negative control, *orfA*. Taken together with dCas9 experiments in *E. coli*, these data demonstrate the utility of the AcrIIA2 and AcrIIA4 proteins to inhibit the function of an orthologous Cas9 in heterologous hosts. These reagents, therefore, represent new tools in the CRISPR-Cas9 genome engineering toolkit.

DISCUSSION

Phage-encoded inhibitors of bacterial immune systems emerge due to the strong selective pressures in the evolutionary arms race between these two entities (Samson et al., 2013). The first identification of phage encoded anti-CRISPRs in type I CRISPR-Cas systems hinted that more CRISPR-Cas inhibitors existed, but methods were lacking for their discovery. Here, we present a bioinformatics strategy that uses “self-targeting” as a genomic marker for CRISPR-Cas inhibitor genes (Figure 1A). This approach led to the identification of four different type II-A CRISPR-Cas9 inhibitors (Figure 3 and 4A), which are collectively present in half of all Cas9-encoding *L. monocytogenes* genomes, including all genomes with self-targeting (Figure 4C). We anticipate that this approach will be helpful for identifying *acr* genes in other CRISPR-Cas systems, although a distinct mechanism for tolerance of self-targeting has been described for type III systems (Goldberg et al., 2014; Samai et al., 2015).

To facilitate the identification of AcrIIA proteins, we first demonstrate a functional CRISPR-Cas9 system in *L. monocytogenes* (Figure 2B). Previous studies of CRISPR-Cas in this organism have focused on the type I-B system and an associated orphan CRISPR array lacking *cas* genes (Mandin et al., 2007; Sesto et al., 2014). Although no canonical CRISPR-Cas function had been established for either system previously, the orphan array was shown to be processed by a host ribonuclease to generate non-coding RNAs (Mandin et al., 2007; Sesto et al., 2014). To observe function for the type II-A CRISPR-Cas system, we used a standard transformation efficiency assay, showing that CRISPR-Cas9 function in strain 10403s is able to limit transformation of a plasmid in a sequence specific manner (Figure 2A and 2B). Given the small colony phenotype observed during transformation of 10403s with the targeted plasmid (pT), we suspect that endogenous levels of *cas9* expression are not sufficient to totally clear the plasmid. Either a small fraction of cells retain the plasmid, or alternatively, cells temporarily possess the plasmid at a reduced copy number, resulting in the small colony phenotype. Consistent with low endogenous expression of *cas9* leading to either form of incomplete plasmid clearance, increased expression of *cas9* resulted in an elimination of detectable transformants in this assay (Figure 2B).

Among the strains with self-targeting, we selected J0161 for further analysis. Using the transformation efficiency assay, we observed no plasmid targeting in this strain (Figure 2C), an observation consistent with the presence of an inhibitor. Indeed, the immune system was inactivated when the ϕJ0161a prophage was transferred to the CRISPR-Cas9-active strain 10403s (Figure 2D). Furthermore, we observed that ϕJ0161a can inactivate CRISPR-Cas9 function in a strain that overexpresses Cas9 (Figure 2E). Mechanistically, this demonstrates that inhibitors are unlikely to function by disrupting the transcriptional regulation of Cas9 and are sufficiently expressed from the integrated prophage to cope with enhanced Cas9 levels.

To identify candidate anti-CRISPR genes, related prophages from CRISPR-active strain 10403s and a prophage that inhibits CRISPR-Cas9 from strain J0161 were compared, and a process-of-elimination cloning approach was taken (Figure 3A). Two isolated *acr* genes (*acrIIA1* and *acrIIA2*) were first identified in ϕJ0161a (Figure 3B). In searching for more anti-CRISPRs, we find that conserved genomic positioning in related phages is a good proxy

for identifying distinct type II-A Cas9 inhibitor proteins, despite a lack of sequence conservation between the proteins themselves (Figure 4A). This has been observed previously in studies of Type I-F and I-E anti-CRISPRs (Bondy-Denomy et al., 2013; Pawluk et al., 2014). In *L. monocytogenes*, the high prevalence of Cas9 inhibitors in prophages suggests the widespread inactivation of CRISPR-Cas9 function (Figure 4C). At present, we do not understand whether there is a mechanistic link to explain the common co-occurrence of *acrIIA1* with other anti-CRISPRs (Figure 4A and 4B). Although this gene is sufficient to inactivate CRISPR-Cas9 function in a plasmid challenge assay, we speculate that it could act as a co-factor or regulator of other *acrIIA* genes during infection or lysogeny, thus explaining the genomic associations observed. Future work will be necessary to understand whether AcrIIA1 is, in fact, a bi-functional protein in this regard and more broadly, whether its superfamily is a marker for *acr* genes.

Phylogenetic analyses demonstrate common occurrences of *acrIIA2-4* in mobile elements in *Listeria* mobile elements (Figure 5). Inhibiting the adaptive immune system likely aids horizontal gene transfer in this organism by blocking Cas9-based targeting and adaptation (Heler et al., 2015). In addition to the family of prophages where these *acrIIA* genes were first identified, homologs were also found in distant siphophages, myophages and plasmids (Supplementary Table 1). Most notably, the *acrIIA4* homologs encoded by virulent myophages did not have *acrIIA1* superfamily homologs in their vicinity. Furthermore, the presence of *acrIIA1* and *acrIIA3* homologs in genera outside of *Listeria* demonstrates that CRISPR-Cas9 inactivation may be common-place in the Firmicutes.

Many potential mechanisms could explain CRISPR-Cas9 inactivation. In their native hosts, *L. monocytogenes,* we have defined anti-CRISPRs by their ability to inhibit Lmo Cas9-based targeting of a plasmid. Furthermore, by demonstrating the efficacy of *acrIIA2* and *acrIIA4* in heterologous hosts with engineered elements (i.e. *cas9* promoter, sgRNA design and promoter) we conclude *acr*-mediated transcriptional repression of the CRISPR-Cas9 system is unlikely. Using the orthologous Spy Cas9, it is clear that AcrIIA2 and AcrIIA4 have broad specificity, given that Lmo Cas9 and Spy Cas9 only share 53% sequence identity. AcrIIA2 and AcrIIA4 likely target regions conserved between the two Cas9 proteins. Type I anti-CRISPRs function by binding directly to the Cas proteins required for target interference and preventing DNA binding or DNA cleavage (Bondy-Denomy et al., 2015). By extension, we expect a similar mechanism for AcrIIA2 and AcrIIA4, given their ability to function in heterologous hosts. The enhanced efficacy of *acrIIA2* in the cleavage-based Cas9 assay relative to the dCas9 based assay suggests that it may inhibit both binding and cleavage to some degree, with cleavage inhibition manifesting as a full inactivation of Cas9 function. However, comparing the results of these two experiments, it is important to note the differences between the stability of Cas9 and dCas9 interactions with the mammalian and bacterial genomes, respectively. Given the efficacy of AcrIIA4 in blocking dCas9-based function (Figure 6B), stable DNA-binding is likely inhibited, although whether this is through a direct interaction with Cas9 remains to be seen.

The identification and future mechanistic dissection of type II-A inhibitors will provide valuable new reagents for studying canonical CRISPR-Cas9 function in natural and engineered settings. The ability of AcrIIA proteins to block Spy Cas9 in *E. coli* and human

cells suggests that these proteins can provide a post-translational “off-switch” for Cas9. This could add a layer of regulation on this powerful system that can be applied in eukaryotic systems to control genome engineering. This new addition to the CRISPR-Cas9 toolbox could enable new applications, such as specifically reversing the effects of dCas9 binding to a genomic locus, or limiting the amount of time that Cas9 is active in the nucleus to reduce off-target gene editing. It will be important to continue to exploit the abundant tools provided to us from the phage-bacteria arms race as we expand the search for inhibitor proteins.

STAR METHODS

CONTACT FOR REAGENT AND RESOURCE SHARING

Please direct any requests for further information or reagents to the lead contact, Joseph Bondy-Denomy (joseph.bondy-denomy@ucsf.edu), Department of Microbiology and Immunology, University of California, San Francisco.

EXPERIMENTAL MODEL AND SUBJECT DETAILS

Microbes—*Listeria monocytogenes* strains were cultured on Brain-Heart Infusion (BHI) medium. *Escherichia coli* strains were cultured on LB medium.

Cell lines—Human Embryonic Kidney 293 plus T cell antigen (HEK293T, CRL-3216, ATCC) cells were cultured in Dulbecco’s Modified Eagle’s Medium (DMEM) supplemented with 10% fetal bovine serum (FBS, Atlanta Biologicals) and 50μg/mL penicillin/streptomycin (P/S, UCSF CCF).

METHOD DETAILS

Assay of CRISPR-Cas9 in *L. monocytogenes*

Plasmid-transformation assay of CRISPR-Cas9: Targeted (pT; pNT for J0161; pRAU31) and non-targeted (pNT; pT_{J0161}; pRAU29) plasmids for *L. monocytogenes* 10403s were constructed by ligating annealed primer pairs into the HindIII and BamHI sites of pKSV7. See Table S3 for plasmid-insert sequences. *L. monocytogenes* strains were transformed with 0.5–1.0 μg pT or pNT by electroporation. Electrocompotent cells were prepared and transformed as described (Park and Stewart, 1990; Zemansky et al., 2009). Transformations were diluted 10-fold into BHI and recovered for two hours, shaking at 30°C. Recovered cultures were plated on BHI with 1.5% agar and 7.5 μg/ml chloramphenicol to select for pT or pNT. For pPL2oexL integrants, tetracycline selection (2 μg/ml) was maintained throughout the procedure, with exception to recovery cultures, which were performed without selection. Whereas plates that contained only chloramphenicol were incubated at 30°C for 36–40 hours prior to imaging, plates that also contained tetracycline were incubated at 30°C for 64–72 hours. Plate images were collected using the Gel Doc™ EZ Gel Documentation System (BioRad) and Image Lab (BioRad) software.

Construction of pPL2oexL-integrants in L. monocytogenes 10403s: The pPL2oexL plasmid for constitutive chromosomal expression of genes in *L. monocytogenes* was derived from pPL2 (Lauer et al., 2002) (See Figure S6). Individual genes or phage fragments were

PCR-amplified from genomic DNA and cloned into pPL2oexL by Gibson Assembly. pPL2oexL-derivative plasmids were electroporated into nonlysogenic 10403s, using a procedure like that which was employed for the plasmid-transformation assay of CRISPR-Cas9 (see text under previous heading). Transformations were recovered for two hours, shaking at 37°C and were plated on BHI-agar with 2 μg/ml tetracycline. Colonies emerged after 36–48 hours incubating at 37°C, and were re-streaked once on the same selective medium to ensure genotypic homogeneity.

Construction of a 10403s::ϕJ0161a lysogen: Phage was induced from *L. monocytogenes* strain J0161 by exposure to ultraviolet radiation as described previously (Loessner and Busse, 1990). 10403s::ϕJ0161a lysogens were isolated from plaques that resulted from spotting amplified J0161 phage stock on a lawn of nonlysogenic 10403s (suspended in BHI with 0.7% agar and 2.5 mM $CaCl_2$). Plaques emerged after 16 hours incubation at 30°C. Lysogeny was confirmed by PCR, as described (Lauer et al., 2002).

Construction of markerless chromosomal deletion strains: Markerless deletions of *cas9* and *acrIIA1-2* were constructed by allelic exchange in nonlysogenic 10403s and 10403s::ϕJ0161a, respectively. Up- and down-stream (700–1000 base pairs) regions flanking the genes to be deleted were fused by overlap-extension PCR and ligated into pKSV7. The Δ*cas9* genotype was inserted between the HindIII and BamHI restriction sites, whereas the Δ*acrA1-2* genotype was inserted between the SacI and BamHI restriction sites. Knockout vectors were transformed by electroporation. Subsequent manipulations were performed as previously reported (Camilli et al., 1993).

Bioinformatic analyses

Identification of self-targeting CRISPR-Cas systems: *L. monocytogenes* genome sequences were downloaded from NCBI. Type-IIA CRISPR arrays were identified within individual genomes using CRISPRfinder (Grissa et al., 2007) or CRISPRDetect (Biswas et al., 2016) web utilities. See Figure S1B for a representative *L. monocytogenes* type II-A CRISPR array. Self-targeting CRISPR-Cas systems were identified using the CRISPRtarget web utility (Biswas et al., 2013) by searching individual *L. monocytogenes* genomes with their own CRISPR arrays. Bona fide self-targeting events were defined as perfect matches lacking spacer-protospacer mutations in the PAM-proximal region (20 bp), concurrent with a cognate PAM sequence (5′-NGG-3′). See Table S1 for a list of self-targeting strains.

Phylogenetic reconstruction of AcrIIA protein families: AcrIIA2- (AEO04363.1), AcrIIA3- (CBY03209.1) and AcrIIA4- (AEO04689.1) homologous protein sequences were acquired by BLASTp searches of all the non-redundant protein sequence database of NCBI on November 5, 2016. Full length (>78% query coverage) sequences of high homology (E value < 1e-04) were downloaded and aligned using Muscle (Edgar, 2004) in MEGA6 (Tamura et al., 2013). Phylogenetic reconstructions of each protein family were performed in MEGA6 using the neighbor-joining method with the Poisson model for amino acid substitution, uniform rates among sites and pairwise deletion of gaps. Reconstructions were tested using the bootstrap method (1000 replications). Reconstruction images were then edited for clarity in Illustrator (Adobe). AcrIIA1- (AEO04364.1) homologous protein

sequences were acquired by four iterations of psiBLASTp searches of the non-redundant protein sequence database of NCBI on October 26, 2016. The position-specific scoring matrix (PSSM) was enchriched with all full-length (>80%) protein sequences. Sequences were downloaded, aligned and reconstructed using the same methodology that was employed for the analysis of AcrIIA2, 3 and 4 (see above). However, in the case of AcrIIA1, sequences with large insertions (>30 amino acids) were removed from the sequence alignments, prior to phylogenetic reconstruction.

Analysis of gene-conservation patterns: The conservation of *acrIIA1*, *acrIIA2*, *acrIIA3*, *acrIIA4* and *cas9* were catalogued in reference to a control gene (cysteinyl-tRNA synthetase) that occurs once in all *L. monocytogenes* genomes. BLASTp searches were performed to acquire lists of genome-specific accession numbers for encoded proteins. These were used as surrogates for genes to assess conservation. Lists were compiled into a single table and sorted so that individual rows of data included accession numbers for all proteins of interest encoded within a single genome.

Inhibition of *Spy*-CRISPRi in *E. coli*

Reporter strain construction: Our *E. coli* Spy-CRISPRi reporter system uses integrated components of the previously reported CRISPRi system (Qi et al., 2013) with minor modifications. The promoter for *mrfp* was modified in the entry vector by changing the promoter from PLlacO-1 to a minimal synthetic promoter (BBa_J23119) (http://parts.igem.org/), PCR amplified, and integrated into BW25113 at *nfsA* by recombineering as described. The *mrfp*-targeting sgRNA was cloned into the site-specific integrating plasmid pCAH63 under control of PLlacO-1 to generate pCs550-r, and integrated at lambda att using the helper plasmid pINT-ts (Haldimann and Wanner, 2001), selecting for chloramphenicol resistance. Conjugation was used to move a chromosomal *dcas9* cassette into recipient strains harboring *mrfp*, sgRNA or both. A “pseudo-Hfr” strain isogenic with BW25113, carries the transfer region from F and a spectinomycin marker integrated downstream of *rhaM* (4086kb) (Typas et al., 2008). A “pseudo-Hfr” *dcas9* donor strain was constructed by integrating *dcas9* and a gentamycin resistance marker at the Tn7 att site (Choi et al., 2005), adjacent to the origin of transfer. *dcas9* was cloned from pdCas9-bacteria (Addgene #44249) under control of BBa_J23105 (http://parts.igem.org/). Putative Cas9 inhibitor proteins were cloned into pBAD24 (Guzman et al., 1995) by Gibson Assembly (NEB) and transformed into the *Spy*-CRISPRi strains by electroporation.

Flow cytometry: Strains were grown overnight in LB with arabinose in deep 96-well plates, and then back-diluted 1:400 into fresh LB with arabinose (to maintain expression of the inhibitor) and IPTG (to induce expression of the sgRNA). After 2.5hr growth (OD~0.4) cultures were fixed using 1.5% final formaldehyde and quenched with glycine, and then diluted 1:30 into phosphate buffered saline. Red fluorescence levels were measured using an LSRII flow cytometer (BD Biosciences) using the yellow/green laser (561 nm) and the PE-Texas Red® detector (610/20 nm). Data for at least 20,000 cells were collected, and median fluorescence values were extracted using FlowJo (FlowJo, LLC). Error bars represent the standard deviation from 3 or more biological replicates. Data from representative samples were plotted as histograms using FlowJo.

Inhibition of Cas9 cleavage in human cells—An eGFP-targeting crRNA was ordered as complementary single-stranded DNA oligos (IDT) and cloned into BbsI linearized pX330 (Addgene, Zhang lab) to generate a single vector expressing S. pyrogenes Cas9-NLS and an eGFP-targeting CRISPR cassette. One candidate (orf) and three validated (acr) acrIIA genes were codon-optimized for human cell expression, synthesized in vitro (IDT, GeneBlock), and cloned into BamHI/EcoRI linearized pcDNA3.1(+) by Gibson assembly. Similarly, the gene encoding enhanced Green Fluorescent Protein (eGFP) was synthesized and cloned into BamHI/EcoRI linearized pLVX-TetOne-Puro (Clontech). Doxycycline-inducible eGFP lentivirus was produced in Human Embryonic Kidney (HEK)293T cells (ATCC) by cotransfection (polyJet, SignaGen) with Gag-Pol packaging construct and VSV-G envelope (pMD2.G, Addgene). Lentiviruses were precipitated from the cellular supernatant at 4°C by incubation in a final concentration of 8.5% Poly(ethylene glycol) average Mn 6000 (PEG-6000) and 0.3M NaCl for 4 hours. Viruses were concentrated at 3500 RPM for 20 minutes in a spinning bucket rotor, suspended in 1 mL 1xPBS, and preserved at −80. One-thousandth viral preparation by volume was used to transduce 250,000 HEK293T cells and successful integrants purified by selection in 1 μg/mL puromycin for 48 hours.

Polyclonal HEK293T cells with a chromosomally-integrated, inducible eGFP cassette were expanded, plated, and transfected with the eGFP-targeting CRISPR construct and each of the bacteriophage genes at different ratios in triplicate (Trans-IT, Mirus). An empty vector was used to equalize the total mass of transfected plasmid across each sample. 36 hours after transfection, cells were treated with 2 μg/mL doxycycline to induce eGFP expression. 12 hours later, cells were suspended by incubation in PBS-EDTA, fixed in 1% formaldehyde PBS, and percent eGFP-positive cells monitored by flow cytometry (FACSCalibur, Gladstone Flow Cytometry Core). Data was normalized to no sgRNA controls and presented as the average percent eGFP-positive cells +/− standard deviation.

QUANTIFICATION AND STATISTICAL ANALYSIS

All experiments were conducted with at least three biological replicates (N >= 3). Statistical parameters are reported in the Figures and the Figure Legends. Additional statistical tests were not performed.

DATA AND SOFTWARE AVAILABILITY

The accession numbers, locus tags and coding sequences for individual genes tested for CRISPR-Cas9 inhibition activity are disclosed in Figure S3. Additional accession numbers for AcrIIA homologs are reported in Table S1.

KEY RESOURCES TABLE

REAGENT or RESOURCE	SOURCE	IDENTIFIER
Experimental Models: Cell Lines		
HEK293T	ATCC	N/A
Experimental Models: Organisms/Strains		

REAGENT or RESOURCE	SOURCE	IDENTIFIER
Listeria monocytogenes 10403s	Laboratory of Daniel Portnoy	ncbi.nlm.nih.gov/Taxonomy/Browser/wwwtax.cgi?mode=Info&id=393133&lvl=3&lin=
Listeria monocytogenes 10403s derivatives	this paper	see Table S2
Listeria monocytogenes J0161	Laboratory of Martin Wiedmann	ncbi.nlm.nih.gov/Taxonomy/Browser/wwwtax.cgi?id=393130
Listeria monocytogenes SLCC2482	Ariane Pietzka	ncbi.nlm.nih.gov/Taxonomy/Browser/wwwtax.cgi?id=863767
Listeria monocytogenes SLCC2540	Ariane Pietzka	ncbi.nlm.nih.gov/Taxonomy/Browser/wwwtax.cgi?id=879089
Escherichia coli BW25113 derivatives	this paper	see Table S2
Recombinant DNA		
pBAD24	Laboratory of Carol Gross	ncbi.nlm.nih.gov/nuccore/X81837.1
pBAD24-derivative plasmids	this paper	see Table S2
pdCas9-bacteria	Addgene	addgene.org/vector-database/44249/
pLVX-TetOne-Puro	Clontech	clontech.com/US/Products/Inducible_Systems/TetSystems_Product_Overview/Tet-One_
pMD2.G	Addgene	addgene.org/12259/
pX330	Addgene	addgene.org/vector-database/42230/
pcDNA3.1(+)	Addgene	addgene.org/vector-database/2093/
pKSV7	Laboratory of Daniel Portnoy	addgene.org/26686/
pKSV7-derivative plasmids	this paper	see Table S2
pPL2oexL	Laboratory of Daniel Portnoy	see Figure S6
pPL2oexL-derivative plasmids	this paper	see Table S2
Sequence-Based Reagents		
GeneBlocks for HEK293T expression of phage proteins	IDT	see Table S3
Software and Algorithms		
Prism 5	GraphPad	graphpad.com/scientific-software/prism/
CRISPRfinder	I2BC	crispr.i2bc.paris-saclay.fr/Server/
CRISPRDetect	Univsersity of Otago	brownlabtools.otago.ac.nz/CRISPRDetect/predict_crispr_array.html
CRISPRtarget	Univsersity of Otago	bioanalysis.otago.ac.nz/CRISPR Target/crispr_analysis.html
illustrator	adobe	adobe.com/Illustrator
MEGA6	MEGA	megasoftware.net/
Image Lab 5.2.1	BioRad	bio-rad.com/en-cn/product/image-lab-software
FlowJo	FlowJo LLC	flowjo.com/

Supplementary Material

Refer to Web version on PubMed Central for supplementary material.

Acknowledgments

We would like to thank Aaron T. Whiteley and Daniel A. Portnoy (UC Berkeley) for providing the prophage-cured and wild type strains of *L. monocytogenes* 10403s as well as plasmids pKSV7 and pPL2oexL. We also acknowledge Martin Wiedmann (Cornell University) for providing strain J0161 and Ariane Pietzka (Austrian Agency for Health and Food Safety) for providing SLCC2482 and SLCC2540. We acknowledge Carol Gross' lab (UCSF) for providing the pBAD24 plasmid and for productive conversations about the project. We specifically thank Carol Gross and Adair Borges for critical reading of the manuscript and thoughtful advice. J.B.D. was supported by the University of California, San Francisco Program for Breakthrough in Biomedical Research, funded in part by the Sandler Foundation, and an NIH Office of the Director Early Independence Award (DP5-OD021344). M.R.S. was supported by National Science Foundation No. 1144247. J.F.H. was supported by an amFAR Mathilde Krim Fellowship, an NIH Human Immunology Project Consortium Infrastructure Pilot (N.J.K, U19 AI118610), and NIH funding for the UCSF-Gladstone Institute of Virology & Immunology Center for AIDS Research (N.J.K., P30 AI027763).

References

Abudayyeh OO, Gootenberg JS, Konermann S, Joung J, Slaymaker IM, Cox DBT, Shmakov S, Makarova KS, Semenova E, Minakhin L, et al. C2c2 is a single-component programmable RNA-guided RNA-targeting CRISPR effector. Science. 2016:aaf5573. [PubMed: 27256883]

Barrangou R, Doudna JA. Applications of CRISPR technologies in research and beyond. Nature Biotechnology. 2016; 34:933–941.

Biswas A, Gagnon JN, Brouns SJJ, Fineran PC, Brown CM. CRISPRTarget: bioinformatic prediction and analysis of crRNA targets. RNA Biol. 2013; 10:817–827. [PubMed: 23492433]

Biswas A, Staals RHJ, Morales SE, Fineran PC, Brown CM. CRISPRDetect: A flexible algorithm to define CRISPR arrays. BMC Genomics. 2016; 17:356. [PubMed: 27184979]

Bondy-Denomy J, Pawluk A, Maxwell KL, Davidson AR. Bacteriophage genes that inactivate the CRISPR/Cas bacterial immune system. Nature. 2013; 493:429–432. [PubMed: 23242138]

Bondy-Denomy J, Garcia B, Strum S, Du M, Rollins MF, Hidalgo-Reyes Y, Wiedenheft B, Maxwell KL, Davidson AR. Multiple mechanisms for CRISPR-Cas inhibition by anti-CRISPR proteins. Nature. 2015; 526:136–139. [PubMed: 26416740]

Brouns SJJ, Jore MM, Lundgren M, Westra ER, Slijkhuis RJH, Snijders APL, Dickman MJ, Makarova KS, Koonin EV, van der Oost J. Small CRISPR RNAs Guide Antiviral Defense in Prokaryotes. Science. 2008; 321:960–964. [PubMed: 18703739]

Camilli A, Tilney LG, Portnoy DA. Dual roles of plcA in Listeria monocytogenes pathogenesis. Molecular Microbiology. 1993; 8:143–157. [PubMed: 8388529]

Choi KH, Gaynor JB, White KG, Lopez C, Bosio CM, Karkhoff-Schweizer RR, Schweizer HP. A Tn7-based broad-range bacterial cloning and expression system. Nat Methods. 2005; 2:443–448. [PubMed: 15908923]

Cong L, Ran FA, Cox D, Lin S, Barretto R, Habib N, Hsu PD, Wu X, Jiang W, Marraffini LA, et al. Multiplex Genome Engineering Using CRISPR/Cas Systems. Science. 2013; 339:819–823. [PubMed: 23287718]

Deltcheva E, Chylinski K, Sharma CM, Gonzales K, Chao Y, Pirzada ZA, Eckert MR, Vogel J, Charpentier E. CRISPR RNA maturation by trans-encoded small RNA and host factor RNase III. Nature. 2011; 471:602–607. [PubMed: 21455174]

Di H, Ye L, Yan H, Meng H, Yamasak S, Shi L. Comparative analysis of CRISPR loci in different Listeria monocytogenes lineages. Biochem Biophys Res Commun. 2014; 454:399–403. [PubMed: 25445602]

East-Seletsky A, O'Connell MR, Knight SC, Burstein D, Cate JHD, Tjian R, Doudna JA. Two distinct RNase activities of CRISPR-C2c2 enable guide-RNA processing and RNA detection. Nature. 2016; 538:270–273. [PubMed: 27669025]

Edgar RC. MUSCLE: multiple sequence alignment with high accuracy and high throughput. Nucleic Acids Research. 2004; 32:1792–1797. [PubMed: 15034147]

Edgar R, Qimron U. The Escherichia coli CRISPR system protects from λ lysogenization, lysogens, and prophage induction. J Bacteriol. 2010; 192:6291–6294. [PubMed: 20889749]

Garneau JE, Dupuis M-È, Villion M, Romero DA, Barrangou R, Boyaval P, Fremaux C, Horvath P, Magadán AH, Moineau S. The CRISPR/Cas bacterial immune system cleaves bacteriophage and plasmid DNA. Nature. 2010; 468:67–71. [PubMed: 21048762]

Gilbert LA, Larson MH, Morsut L, Liu Z, Brar GA, Torres SE, Stern-Ginossar N, Brandman O, Whitehead EH, Doudna JA, et al. CRISPR-Mediated Modular RNA-Guided Regulation of Transcription in Eukaryotes. Cell. 2013; 154:442–451. [PubMed: 23849981]

Goldberg GW, Jiang W, Bikard D, Marraffini LA. Conditional tolerance of temperate phages via transcription-dependent CRISPR-Cas targeting. 2014; 514:633–637.

Grissa I, Vergnaud G, Pourcel C. CRISPRFinder: a web tool to identify clustered regularly interspaced short palindromic repeats. Nucleic Acids Research. 2007; 35:W52–W57. [PubMed: 17537822]

Guzman LM, Belin D, Carson MJ, Beckwith J. Tight regulation, modulation, and high-level expression by vectors containing the arabinose PBAD promoter. J Bacteriol. 1995; 177:4121–4130. [PubMed: 7608087]

Haldimann A, Wanner BL. Conditional-replication, integration, excision, and retrieval plasmid-host systems for gene structure-function studies of bacteria. J Bacteriol. 2001; 183:6384–6393. [PubMed: 11591683]

Haurwitz RE, Jinek M, Wiedenheft B, Zhou K, Doudna JA. Sequence- and Structure-Specific RNA Processing by a CRISPR Endonuclease. Science. 2010; 329:1355–1358. [PubMed: 20829488]

Heler R, Samai P, Modell JW, Weiner C, Goldberg GW, Bikard D, Marraffini LA. Cas9 specifies functional viral targets during CRISPR-Cas adaptation. Nature. 2015; 519:199–202. [PubMed: 25707807]

Jinek M, Chylinski K, Fonfara I, Hauer M, Doudna JA, Charpentier E. A Programmable Dual-RNA-Guided DNA Endonuclease in Adaptive Bacterial Immunity. Science. 2012; 337:816–821. [PubMed: 22745249]

Labrie SJ, Samson JE, Moineau S. Bacteriophage resistance mechanisms. Nat Rev Micro. 2010; 8:317–327.

Lauer P, Chow MYN, Loessner MJ, Portnoy DA, Calendar R. Construction, characterization, and use of two Listeria monocytogenes site-specific phage integration vectors. J Bacteriol. 2002; 184:4177–4186. [PubMed: 12107135]

Loessner MJ, Busse M. Bacteriophage typing of Listeria species. Applied and Environmental Microbiology. 1990; 56:1912–1918. [PubMed: 2116763]

Makarova KS, Wolf YI, Alkhnbashi OS, Costa F, Shah SA, Saunders SJ, Barrangou R, Brouns SJJ, Charpentier E, Haft DH, et al. An updated evolutionary classification of CRISPR-Cas systems. Nat Rev Micro. 2015; 13:722–736.

Mali P, Yang L, Esvelt KM, Aach J, Guell M, DiCarlo JE, Norville JE, Church GM. RNA-guided human genome engineering via Cas9. Science. 2013; 339:823–826. [PubMed: 23287722]

Mandin P, Repoila F, Vergassola M, Geissmann T, Cossart P. Identification of new noncoding RNAs in Listeria monocytogenes and prediction of mRNA targets. Nucleic Acids Research. 2007; 35:962–974. [PubMed: 17259222]

Marraffini LA. CRISPR-Cas immunity in prokaryotes. Nature. 2015; 526:55–61. [PubMed: 26432244]

Maxwell KL, Garcia B, Bondy-Denomy J, Bona D, Hidalgo-Reyes Y, Davidson AR. The solution structure of an anti-CRISPR protein. Nature Communications. 2016; 7:13134.

Mojica FJM, Díez-Villaseñor C, García-Martínez J, Soria E. Intervening sequences of regularly spaced prokaryotic repeats derive from foreign genetic elements. J Mol Evol. 2005; 60:174–182. [PubMed: 15791728]

Nuñez JK, Kranzusch PJ, Noeske J, Wright AV, Davies CW, Doudna JA. Cas1-Cas2 complex formation mediates spacer acquisition during CRISPR-Cas adaptive immunity. Nat Struct Mol Biol. 2014; 21:528–534. [PubMed: 24793649]

Park SF, Stewart GS. High-efficiency transformation of Listeria monocytogenes by electroporation of penicillin-treated cells. Gene. 1990; 94:129–132. [PubMed: 2121618]

Pawluk A, Bondy-Denomy J, Cheung VHW, Maxwell KL, Davidson AR. A new group of phage anti-CRISPR genes inhibits the type I-E CRISPR-Cas system of Pseudomonas aeruginosa. mBio. 2014; 5:e00896–14. [PubMed: 24736222]

Pawluk A, Staals RHJ, Taylor C, Watson BNJ, Saha S, Fineran PC, Maxwell KL, Davidson AR. Inactivation of CRISPR-Cas systems by anti-CRISPR proteins in diverse bacterial species. Nature Microbiology. 2016; 1:1–6.

Qi LS, Larson MH, Gilbert LA, Doudna JA, Weissman JS, Arkin AP, Lim WA. Repurposing CRISPR as an RNA-guided platform for sequence-specific control of gene expression. Cell. 2013; 152:1173–1183. [PubMed: 23452860]

Ran FA, Cong L, Yan WX, Scott DA, Gootenberg JS, Kriz AJ, Zetsche B, Shalem O, Wu X, Makarova KS, et al. In vivo genome editing using Staphylococcus aureus Cas9. Nature. 2015; 520:186–191. [PubMed: 25830891]

Samai P, Pyenson N, Jiang W, Goldberg GW, Hatoum-Aslan A, Marraffini LA. Co-transcriptional DNA and RNA Cleavage during Type III CRISPR-Cas Immunity. Cell. 2015; 161:1164–1174. [PubMed: 25959775]

Samson JE, Magadán AH, Sabri M, Moineau S. Revenge of the phages: defeating bacterial defences. Nat Rev Micro. 2013; 11:675–687.

Sesto N, Touchon M, Andrade JM, Kondo J, Rocha EPC, Arraiano CM, Archambaud C, Westhof E, Romby P, Cossart P. A PNPase dependent CRISPR System in Listeria. PLoS Genet. 2014; 10:e1004065. [PubMed: 24415952]

Söding J, Biegert A, Lupas AN. The HHpred interactive server for protein homology detection and structure prediction. Nucleic Acids Research. 2005; 33:W244–W248. [PubMed: 15980461]

Tamura K, Stecher G, Peterson D, Filipski A, Kumar S. MEGA6: Molecular Evolutionary Genetics Analysis version 6.0. Mol Biol Evol. 2013; 30:2725–2729. [PubMed: 24132122]

Typas A, Nichols RJ, Siegele DA, Shales M, Collins SR, Lim B, Braberg H, Yamamoto N, Takeuchi R, Wanner BL, et al. High-throughput, quantitative analyses of genetic interactions in E. coli. Nat Methods. 2008; 5:781–787. [PubMed: 19160513]

Wang X, Yao D, Xu J-G, Li A-R, Xu J, Fu P, Zhou Y, Zhu Y. Structural basis of Cas3 inhibition by the bacteriophage protein AcrF3. Nat Struct Mol Biol. 2016; 23:868–870. [PubMed: 27455460]

Wright AV, Nuñez JK, Doudna JA. Biology and Applications of CRISPR Systems: Harnessing Nature's Toolbox for Genome Engineering. Cell. 2016; 164:29–44. [PubMed: 26771484]

Yosef I, Goren MG, Qimron U. Proteins and DNA elements essential for the CRISPR adaptation process in Escherichia coli. Nucleic Acids Research. 2012; 40:5569–5576. [PubMed: 22402487]

Zemansky J, Kline BC, Woodward JJ, Leber JH, Marquis H, Portnoy DA. Development of a mariner-based transposon and identification of Listeria monocytogenes determinants, including the peptidyl-prolyl isomerase PrsA2, that contribute to its hemolytic phenotype. J Bacteriol. 2009; 191:3950–3964. [PubMed: 19376879]

Zetsche B, Gootenberg JS, Abudayyeh OO, Slaymaker IM, Makarova KS, Essletzbichler P, Volz SE, Joung J, van der Oost J, Regev A, et al. Cpf1 Is a Single RNA-Guided Endonuclease of a Class 2 CRISPR-Cas System. Cell. 2015; 163:759–771. [PubMed: 26422227]

HIGHLIGHTS

- Bacteriophage anti-CRISPR proteins AcrIIA1-4 inactivate CRISPR-Cas9
- Half of *L. monocytogenes* isolates possess inhibited CRISPR-Cas9 systems
- AcrIIA2 and AcrIIA4 prevent target binding by dCas9 in bacteria
- AcrIIA2 and AcrIIA4 inhibit Cas9-mediated gene editing in human cells

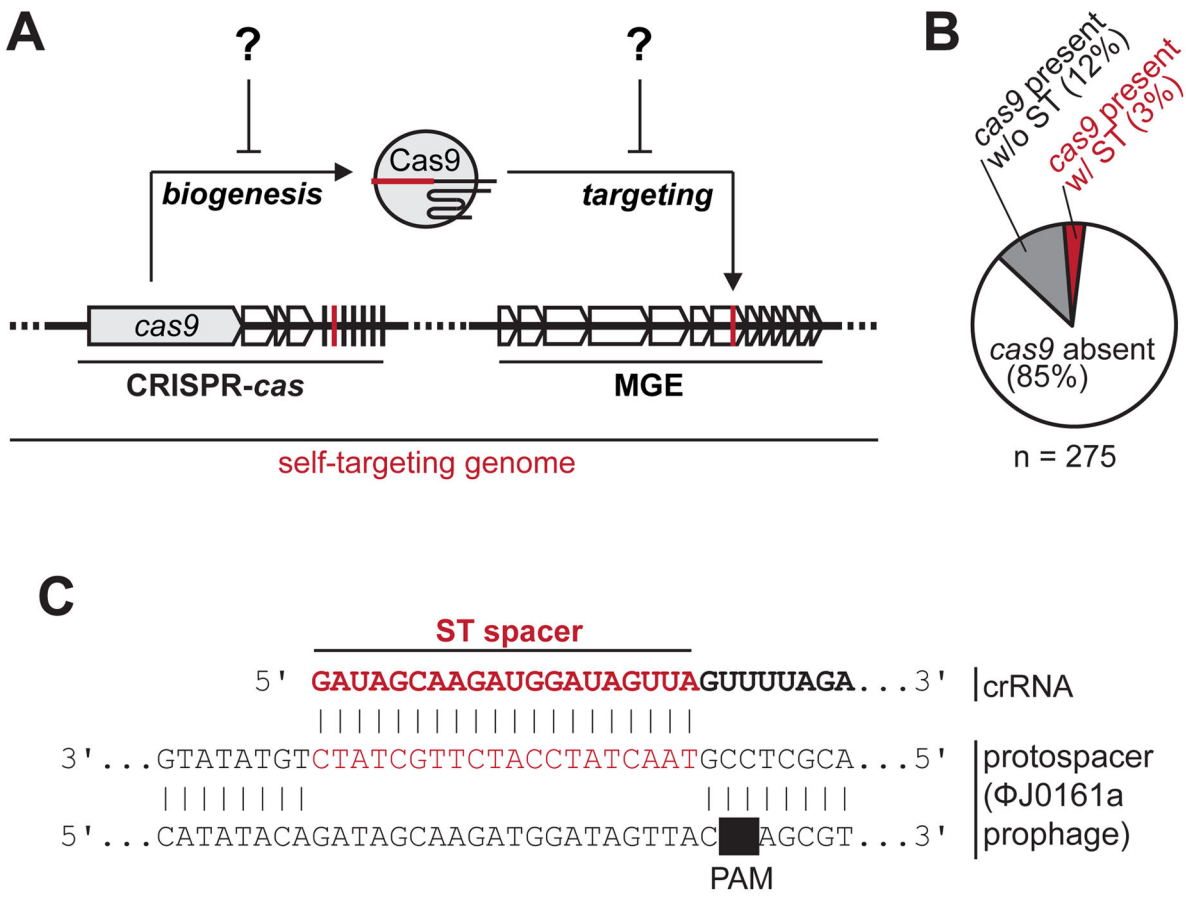

Figure 1. A survey for CRISPR-Cas9 genomic self-targeting (ST) in *Listeria monocytogenes*

(A) A schematic depicting the principle of genomic self-targeting, where a mobile genetic element (MGE) possesses a target sequence for a spacer in a CRISPR array in the same genome. CRISPR-Cas9 function in this “self-targeting genome” is presumably inactive for continued cell viability.

(B) The abundance of genomes with (red) and without (gray) *cas9*-linked self-targeting (ST), in *L. monocytogenes* genomes. See Table S1 for a list of self-targeting strains.

(C) An example of an ST event, where spacer 16 in the type II-A CRISPR array of strain J0161 has a perfect PAM and protospacer match with a resident prophage (ϕJ0161a). See Figure S1B for the entire CRISPR array.

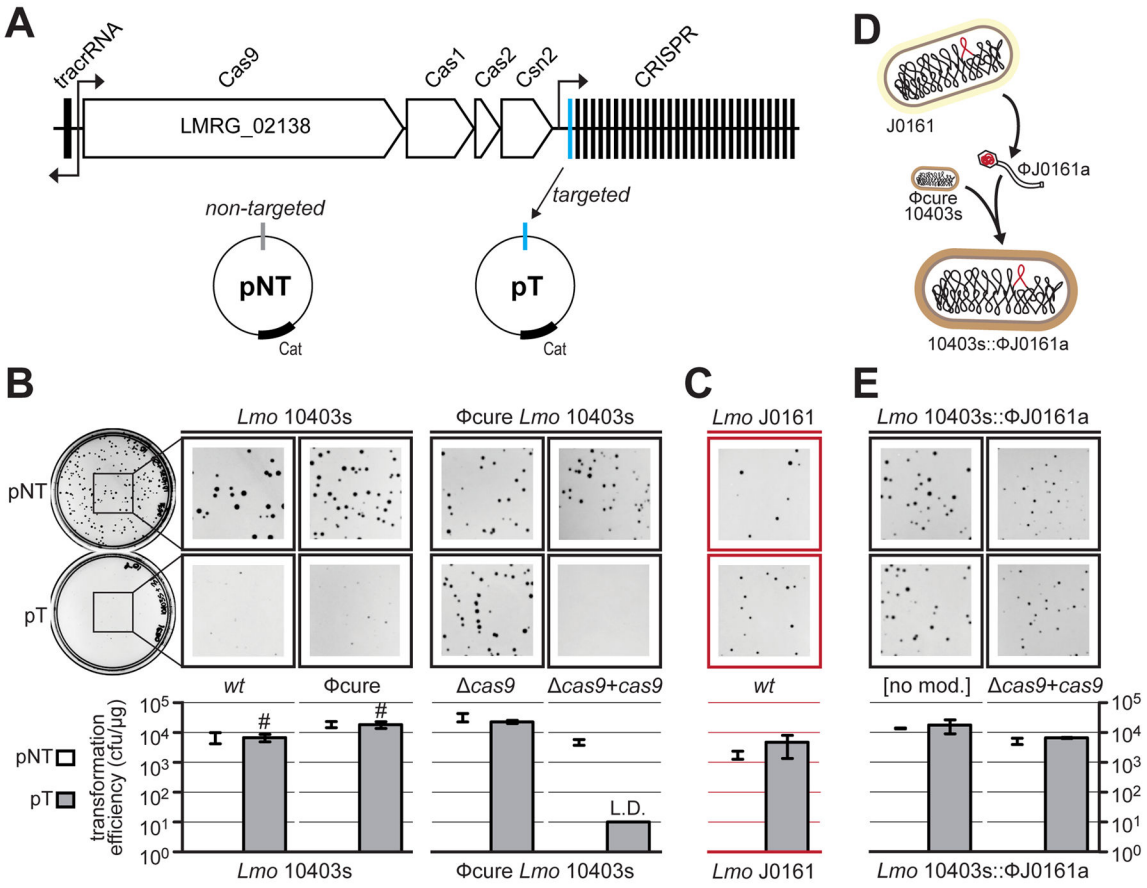

Figure 2. A prophage from *L. monocytogenes* J0161 inhibits CRISPR-Cas9 function

(A) The type II-A CRISPR-Cas locus in *L. monocytogenes* 10403s. Four *cas* genes and the upstream tracrRNA are indicated, along with a CRISPR array containing 30 spacers. The predicted direction of transcription is indicated with black arrows. Subsequent experiments utilize a non-targeted plasmid (pNT) and a targeted plasmid (pT) that has a protospacer matching spacer 1 in this strain.

(B) Representative pictures of colonies of *Lmo* 10403s wild type (wt), prophage-cured (ϕcure), *cas9*-deletion strain (*Δcas9*), and a *cas9* overexpression strain (Δ*cas9* + *cas9)* after being transformed with pT or pNT plasmids. Bar graphs below the plates show the calculated transformation efficiency (colony forming units per μg of plasmid). Data are represented as the mean of three biological replicates +/− SD. L.D. limit of detection, transformants with small colonies denoted with #.

(C) Plasmid-targeting assay with wild type J0161 (contains the ϕJ0161a prophage; experiment conducted as in (B), except with pT_{J0161} as the targeted plasmid) is shown in red to denote self-targeting (as in Figure 1).

(D) A schematic demonstrating the construction of a 10403s strain containing the prophage ϕJ0161a (10403s::ϕJ0161a). See STAR Methods for details. (E) Plasmid-targeting assay with 10403s lysogenized with the ϕJ0161a prophage (10403s::ϕJ0161a) with endogenous (no mod) or overexpressed *cas9* (Δ*cas9* + *cas9*; experiment conducted as in (B)).

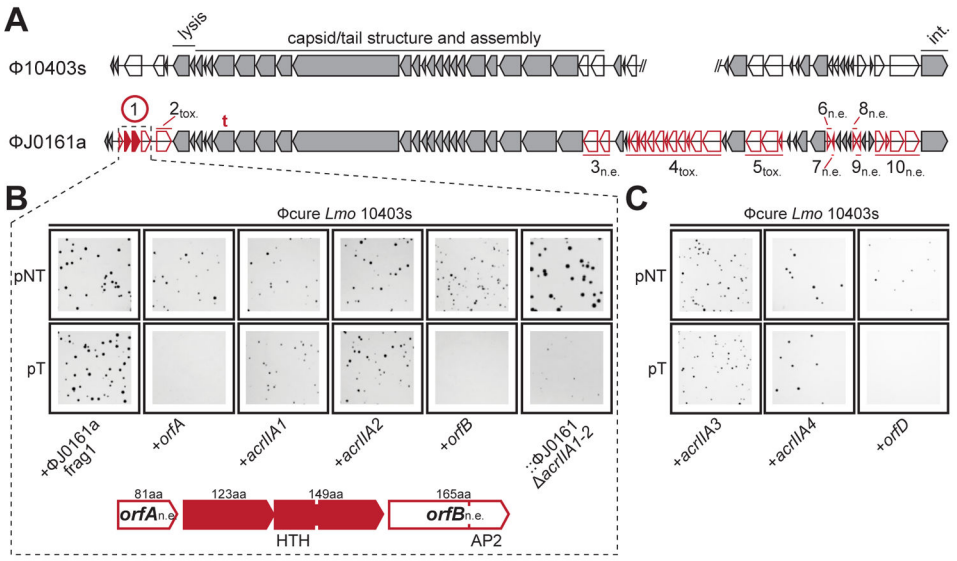

Figure 3. Identification of four distinct anti-CRISPR proteins

(A) Comparison of the open reading frames from two similar prophages from *L. monocytogenes* 10403s and J0161. Unique genes (red) comprising ten fragments of ϕJ0161 were tested for CRISPR-Cas9 inhibition in 10403s. n.e., No effect on CRISPR-Cas9 activity, tox., fragment toxic when expressed, t., location of self-targeted protospacer. The encircled fragment exhibited anti-CRISPR activity with two genes (*acrAII1, acrAII2*) independently capable of inhibiting CRISPR-Cas activity. Conserved (grey) genes were not tested. For reference, phage genes involved in cell lysis, capsid assembly and host integration (int.) are labeled.

(B) Representative colony pictures of Lmo 10403s ϕcure strains constitutively expressing "fragment 1" (as shown in (A)) or the indicated individual genes from ϕJ0161a transformed with pNT or pT. The rightmost panels show a 10403s lysogen of ϕJ0161a with CRISPR-Cas9 inhibitor genes deleted (::ϕJ0161aΔ*acrIIA1-2*). See Figure S2 for data from the other ϕJ0161a fragments and Figure S2/S3 for full plates.

(C) Representative colony pictures of Lmo 10403s ϕcure strains constitutively expressing *acrIIA3, acrIIA4,* or *orfD* transformed with pNT or pT.

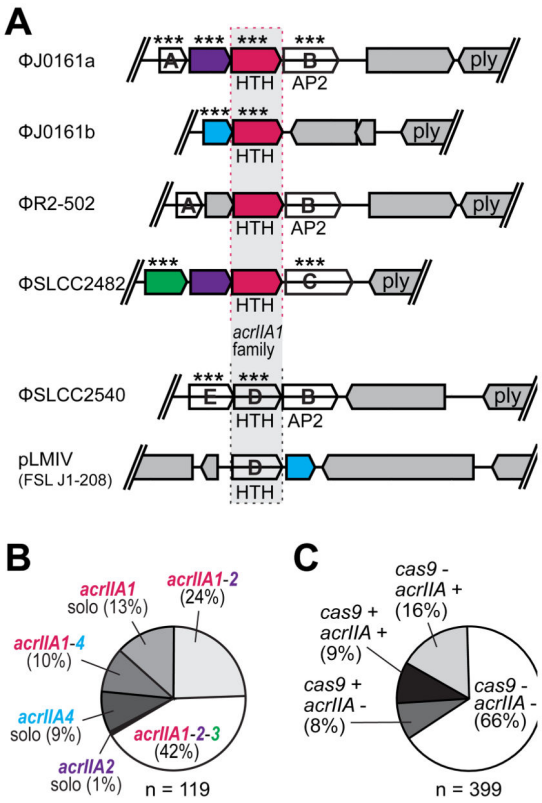

Figure 4. Genomic organization and prevalence of *acrIIA* genes

(A) The genomic context of *acrIIA1* (1) and its homolog from *L. monocytogenes* (*orfD*) are depicted to scale as cartoons with *acrIIA1* homologs in vertical alignment. Typically, *acrIIA* genes are encoded within prophages adjacent to or near the phage lysin (ply) gene. Genomic neighbors of *acrIIA1* and *orfD* (*acrIIA1-4, orfA-E*) are shown. Individual genes (***) were assayed for CRISPR-Cas9 inhibition in *L. monocytogenes* 10403s (see Figure 3 and Figure S3). Helix-turn-helix (HTH) and AP2 DNA binding motifs were detected in some proteins using hidden markov model (HMM) prediction software (Söding et al., 2005).

(B) Pie-graph representation of the frequency of each *acrIIA* gene co-occurrences

(C) Pie-graph representation of the prevalence of *acrIIA* and *cas9* genes in the *L. monocytogenes* pangenome. See Table S1 for relevant accession numbers.

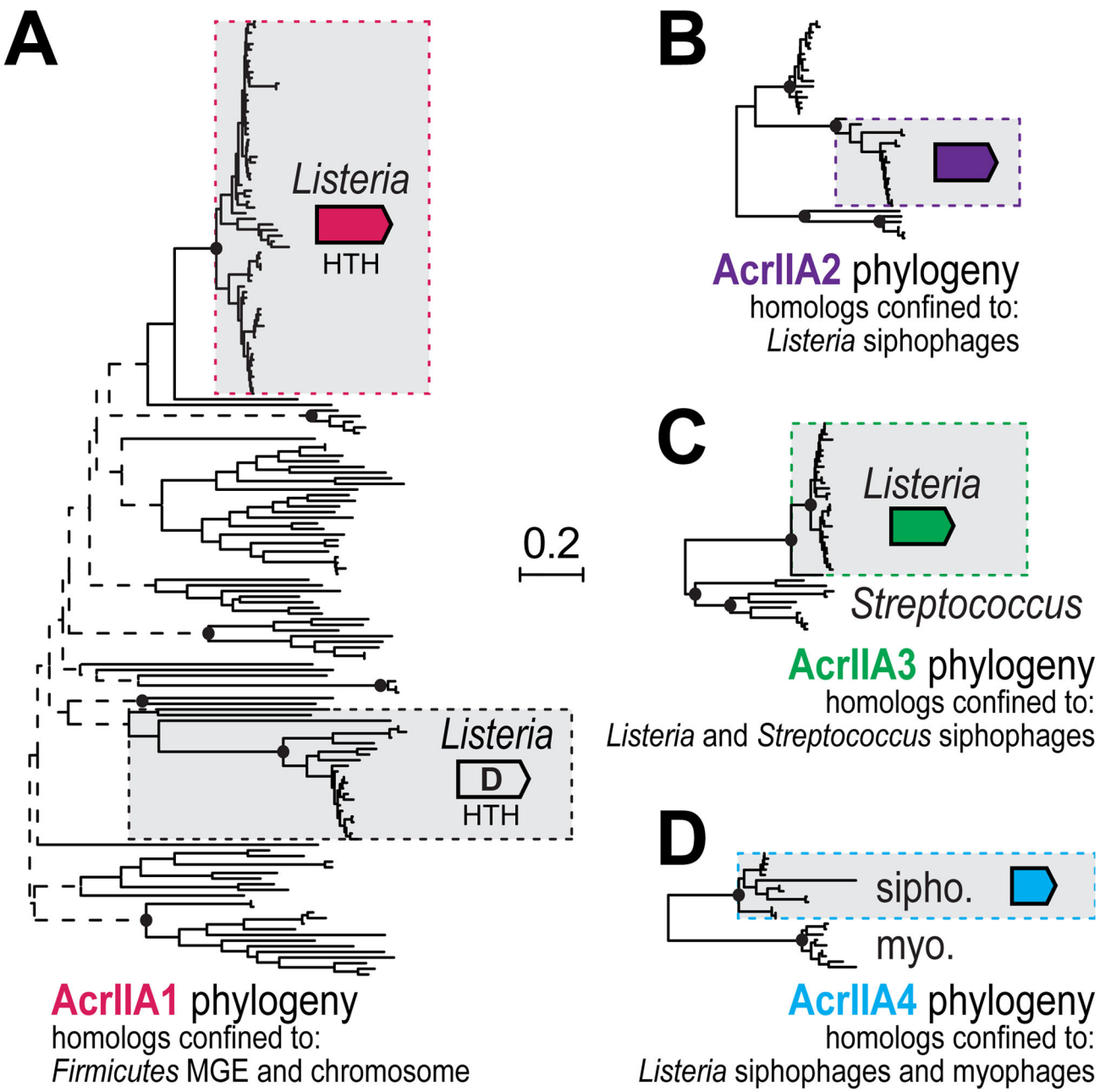

Figure 5. Phylogenetic analysis of AcrIIA1-4 homologs

An unrooted phylogenetic reconstruction of full-length protein sequences identified following an iterative psi-BLASTp search to query all non-redundant protein sequences within GenBank for

(A) AcrIIA1.

BLASTp was used to identify sequences for similar phylogenetic reconstructions of

(B) AcrIIA2,

(C) AcrIIA3,

(D) AcrIIA4 (see STAR Methods). Selected bootstrapping support values are denoted with filled ovals (≥90%), open rectangles (≥70%) or dashed lines (<70%). The sequence family

that is boxed-in represents the family that was tested for anti-CRISPR function. Other homologs reflect distinct sub-families present in the genomes described under the tree.

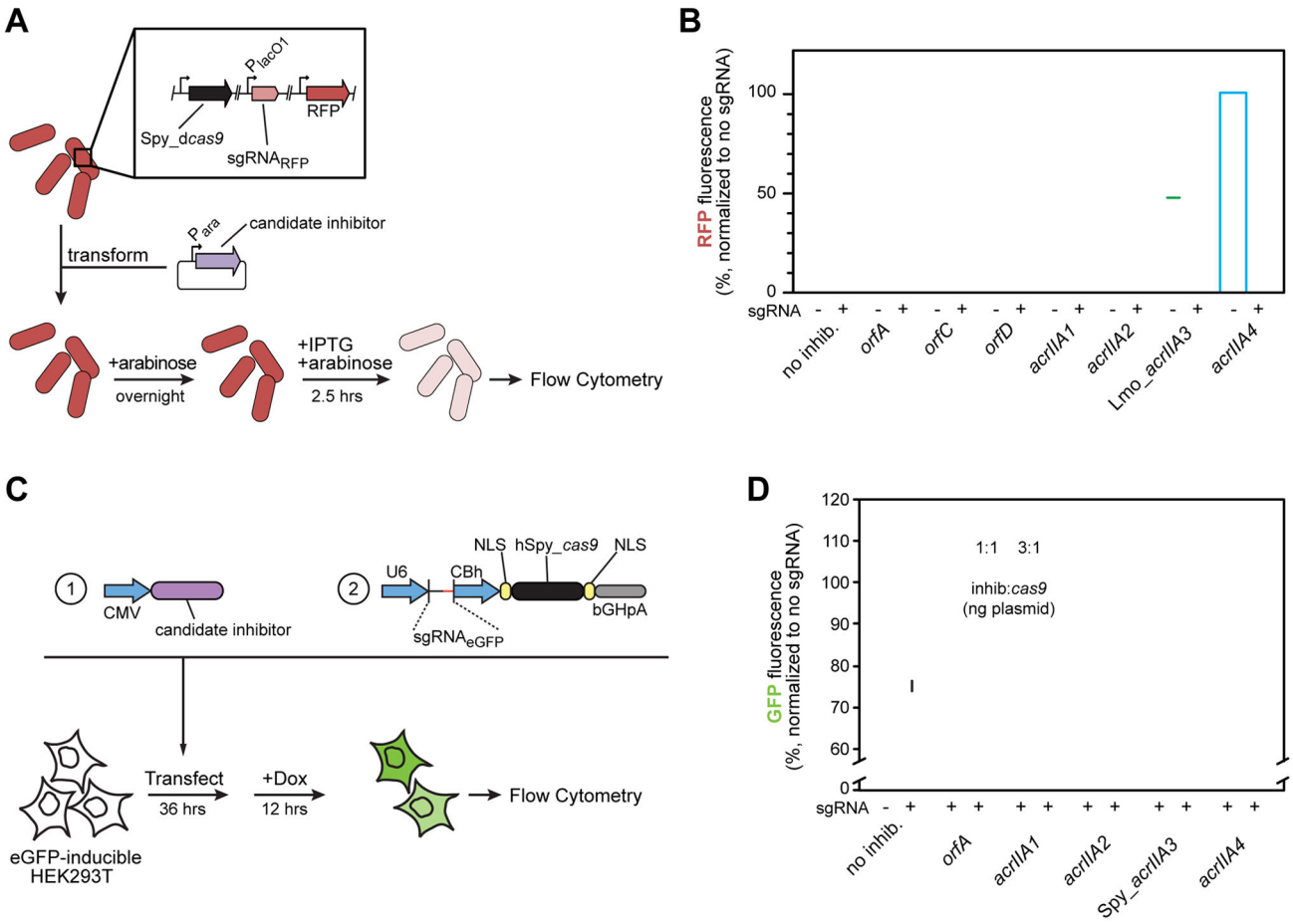

Figure 6. Inhibition of *Streptococcus pyogenes* dCas9 and Cas9

(A) A schematic outlining the experimental setup, where single-cell fluorescence of *E. coli* BW25113 expressing *Streptococcus pyogenes* (Spy) dCas9 and a sgRNA targeted towards a chromosomal red fluorescent protein (RFP) gene was measured by flow cytometry.

(B) Candidate (*orf*) and validated (*acr*) *acrIIA* genes were tested for their ability to inhibit dCas9-based gene repression. Measurements taken reflect the median RFP fluorescence value of a single cell in a unimodal population normalized for each candidate gene to a sgRNA-free control. Error bars represent the mean +/− SD of at least three biological replicates. See Figure 3 and Figure S3 for gene-identification information. See Figure S4 for raw flow cytometry data.

(C) A schematic outlining the experimental setup, where HEK293T cells with a chromosomally-integrated, doxycycline-inducible eGFP cassette were transfected with a plasmid encoding a single transcript tracrRNA/eGFP-targeting sgRNA and NLS-SpyCas9 alongside expression constructs encoding one of five codon-optimized phage genes at different ratios. The percent of eGFP positive cells was measured 12 hours after induction by flow cytometry.

(D) Candidate (*orf*) and validated (*acr*) *acrIIA* genes were tested for their ability to inhibit dCas9-based gene editing. An increasing amount of inhibitor plasmid (in ng) was added from left to right, at a ratio to the Cas9/sgRNA plasmid of 1:1 and 3:1. Data were

normalized to transfection with no phage ORF as the baseline. Average percent of eGFP positive cells is depicted +/− SD across biological triplicates. See Figure S5 for raw flow cytometry data.